Integration of a Quantitative Feedback Theory (QFT)-Based Active Noise Canceller and 3D Audio Processor to Headsets

Mingsian R. Bai
e-mail: msbai@mail.nctu.edu.tw

Jianliang Lin

Department of Mechanical Engineering,
National Chiao-Tung University,
1001 Ta-Hsueh Road,
Hsin-Chu 300, Taiwan

This paper seeks to enhance the quality of spatial sound reproduction by integrating two advanced signal processing technologies, active noise control (ANC) and three-dimensional (3D) audio, to a headset. The ANC module of the headset is designed based on the quantitative feedback theory (QFT), which is a unified theory that emphasizes the use of feedback for achieving the desired system performance tolerances in the face of plant uncertainties and plant disturbances. Performance, stability, and robustness of the closed-loop system have been taken into account in the loop-shaping procedure within a general framework of the QFT. On the other hand, 3D audio processing algorithms including the head-related-transfer-function and the reverberator are realized on the platform of a fixed-point digital signal processor. Listening tests were conducted to evaluate the proposed system in terms of various subjective performance indices. The experimental results revealed that the 3D headset is capable of delivering superior rendering quality of localization and spaciousness, with the aid of the ANC module.
[DOI: 10.1115/1.2748461]

1 Introduction

Three-dimensional (3D) audio has emerged as a new technology to create spatial sound field for a great variety of applications including home theater, multimedia, MP3 player, TV, mobile phones, games, toys, automotive audio, and so forth. However, it frequently occurs that the quality of the sound reproduction can be significantly degraded when the user is exposed to a noisy environment such as streets, stations, shopping centers, and vehicle cabinets. It is then desirable to develop effective methods to address the noise problem before the spatial sound reproduction is implemented. Conventional ways of noise abatement are either to isolate or to dampen the noise source or path by using passive elements, e.g., sound-absorbing materials. Despite the simplicity, conventional methods are known to be ineffective at low frequencies, where required passive elements can become impractically bulky. Therefore, instead of using passive treatments, active noise control (ANC) techniques are employed in the present work to cope with the disturbing noises especially for those at low frequencies. By "active," we mean to cancel the noise using an electronically created counternoise. Among all ANC applications with varying degree of complexity, active headsets are perhaps the most mature and have achieved great commercial success. Active headsets enable quality sound reproduction with reduced background noise level.

An active headset system is proposed in this paper to enhance the quality of spatial sound reproduction by integrating 3D audio processing and ANC. The ANC module of the headset is designed based on the quantitative feedback theory (QFT) [1–3], which is a unified theory that emphasizes the use of feedback for achieving the desired system performance tolerances in the face of plant uncertainties and plant disturbances. Performance, stability, and robustness of the closed-loop system have been taken into account in the loop-shaping procedure within a general framework of the QFT. The feedback controller shall be implemented by using analog circuits to avoid unnecessary delay.

The 3D audio processor aims at producing a sensation of localization using head related transfer functions (HRTF) [4] and a sensation of spaciousness using artificial reverberators. A HRTF is a transformation for a specific source direction relative to the head, which describes the filtering process associated with the diffraction of sound by the torso, head, and pinnae [5–7]. A sound image in the 3D space can be created with the aid of digital filters that simulate the HRTF at the intended direction. Specifically, the filter is usually implemented as a finite impulse response (FIR) filter by using the head-related impulse responses (HRIR), or the inverse Fourier transform of the HRTF. Several HRTF databases are currently available [4,8]. The HRTF database we used for the present work is from the website of the MIT media lab [4].

Reverberation results from the endless reflections of sound waves in a bounded space. As another important element of 3D audio, reverberation carries the cues of human perception to acoustic environment such as the size of room and the absorptivity of the boundary. In audio reproduction and mixing, reverberation is necessary for enriching the dry recording to make it sound more natural and spatial than the original. In some ill-conditioned listening environments, e.g., car cabin, artificial reverberation is also useful in mitigating the coloration problems due to a small space during surround presentation. Reverberation can also be used in the context of headphone rendering to externalize the sound images so that listening discomfort can be minimized.

Listening tests are carried out to compare the performance of 3D audio processing, with and without the ANC, in terms of various subjective indices. The results are post-processed by using the analysis of variance (ANOVA) to assess the statistical significance of the results. The comparison will be summarized in terms of computation cost and subjective performance indices.

2 Active Noise Control

2.1 ANC Overview. The origin of the ANC technique dates back to 1936. It has been an active area in acoustics since Lueg filed his patent [9]. ANC is sound field modification or cancella-

Contributed by the Technical Committee on Vibration and Sound of ASME for publication in the JOURNAL OF VIBRATION AND ACOUSTICS. Manuscript received September 28, 2005; final manuscript received February 26, 2007. Review conducted by Richard F. Keltie.

tion by electro-acoustical means. The name differentiates "active control" from traditional "passive" methods for controlling unwanted sound and vibration. Passive control treatments include insulation, silencers, vibration mounts, damping treatments, absorptive treatments such as ceiling tiles, and conventional mufflers. Passive techniques work best at middle and high frequencies, but can be bulky and heavy when used for low frequencies. In contrast, the light weight and small size of active systems can be attractive, especially for low-frequency applications. Research efforts have been attempted to implement this emerging technology on a great variety of applications, such as headsets [10], active duct silencers, active noise cancellers in vehicles [11] or aircraft [12] cabins, and so forth [13–15]. Among the ANC applications, active headsets can be regarded as the most mature and practical system from a commercial standpoint. A more comprehensive review of ANC technology can be found in Refs. [16,17].

In the study, feedback control structure is adopted for the design of active headsets. The reason for this is partly because the upstream reference is usually unavailable and partly because the system order is sufficiently low for feedback control to be practical in broadband noise rejection. An original design of an active headset can be attributed to Olson and May [18], and also Wheeler [19]. Their designs were based on classical frequency-domain compensation that relies heavily on heuristically shaping the open-loop frequency response with acceptable margins.

2.2 The QFT Technique. Instead of classical loop-shaping that requires much trial and error, a more systematic and efficient approach based on the QFT is employed in the present paper. In the 1960s, as a continuation of the pioneering work of Bode, Horowitz introduced a frequency-domain design methodology [1] that was refined in the 1970s to its present form, commonly referred to as the QFT [2,3]. As a natural extension of classical frequency-domain design approaches, the QFT is an engineering method devoted to practical design of feedback systems.

Control design necessary to accomplish performance specifications in the presence of uncertainties (plant perturbations and/or external disturbances) is a key consideration in the feedback design. In the QFT, one of the main objectives is to design a simple and low-order controller with minimum bandwidth. This distinct feature makes the QFT a practical design method for designing feedback controllers, as compared to other methods that often lead to higher order controllers. Minimum bandwidth controllers are a natural requirement in practice in order to avoid problems with noise amplification, resonances, and unmodeled high-frequency dynamics. In most practical design situations iterations are inevitable, and the QFT offers direct insight into the available tradeoff between controller complexity and specifications during such iterations in an interactive but systematic way.

3 3D Audio Processing

3.1 HRTF. The HRTF relates the transmitted sound pressure of the source to the pressure developed at the ear drum. It varies with frequency, azimuth, elevation, and range, and reveals the physical cues for sound localization. In essence, HRTFs can be associated with the scattering and diffraction pattern around the head due to the incident plane waves. In general, the HRTFs are preprocessed by a normalization procedure of some sort to remove the influence of distance and transducer dynamics. Several HRTF databases are currently available [4,8]. The HRTF database we used for the present work is from the website of the MIT media lab [4].

A sound illusion in the 3D space can be realized by using digital filters that simulate the HRTF at the intended direction. To be specific, the filter is usually implemented as a FIR filter by using the HRIR. Thus, the binaural signals can be produced by straightforward convolution of the source signal with the HRIR of the corresponding ear

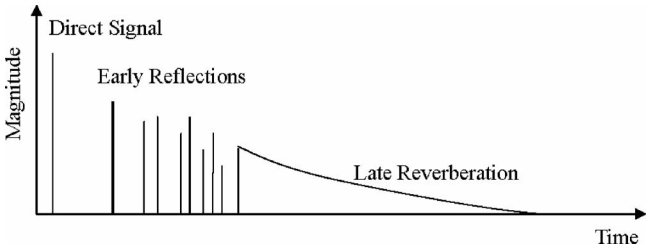

Fig. 1 Schematic diagram of a typical room response

$$x_L(\theta,\phi,n) = \sum_{m=0}^{M-1} h_L(\theta,\phi,m)s(n-m) \tag{1}$$

$$x_R(\theta,\phi,n) = \sum_{m=0}^{M-1} h_R(\theta,\phi,m)s(n-m) \tag{2}$$

where θ and ϕ denote the azimuth and elevation angles, respectively; $s(n)$ is the monophonic source signal at the discrete time index n; $h_L(\theta,\phi,m)$ and $h_R(\theta,\phi,m)$ are the HRIRs (assumed M taps) of the left and right ears, respectively, at the discrete time index m and the intended direction; and $x_L(\theta,\phi,n)$ and $x_R(\theta,\phi,n)$ are the simulated binaural signals. Since the HRTF requires a large amount of memory storage and computing power, previous research has suggests various techniques such as array models and the singular value decomposition (SVD) to ease the processing [20].

3.2 Synthesis of Reverberation. Reverberators are key elements in spatial audio reproduction. The spaciousness of reproduced sound can be enriched by using reverberators. A room response can in general be divided into two parts, as shown in Fig. 1. The early reflection, lasting for approximately 80 ms, is composed of the direct sound accompanied by discrete reflections. Early reflection is dependent on room geometry as well as the relative positions of the source and the receiver. As compared to the early reflection, the late reverberation is less structural and contains extremely dense echoes with exponentially decreasing amplitude. Both parts of the response are highly complex in typical diffuse sound fields and are difficult, if not impossible, to model using modal analysis.

Several statistics of the room response are relevant in the design

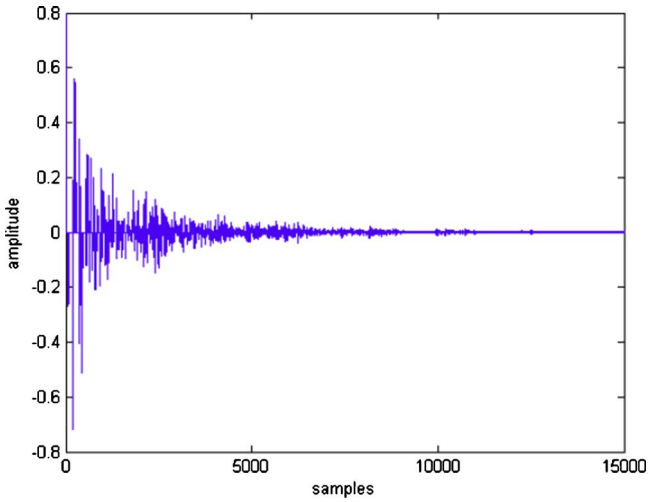

Fig. 2 The impulse response obtained by using the image-source method with 30th-order reflections. The room dimension is 10 m×8 m×3 m and absorption coefficient is 0.8.

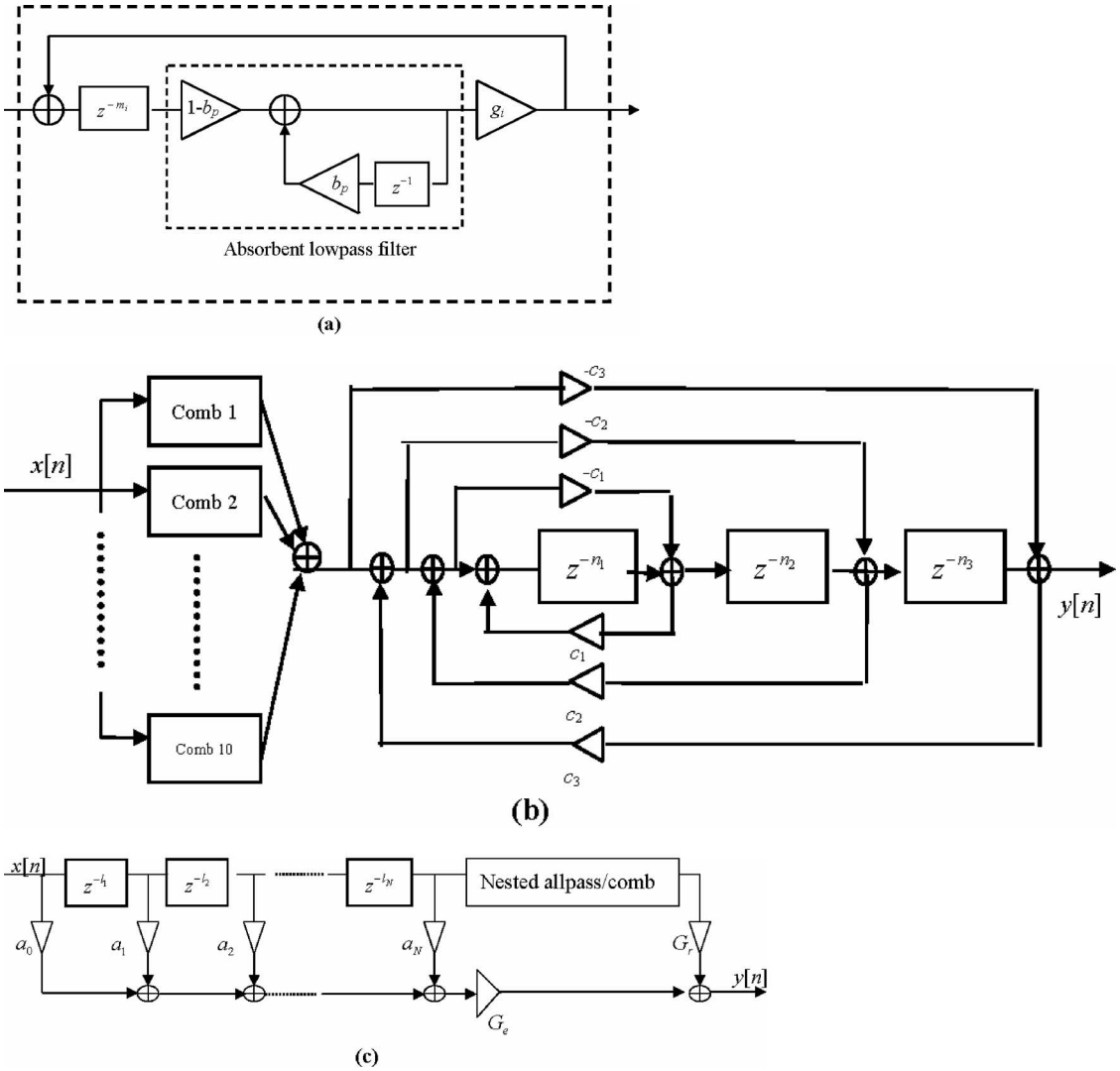

Fig. 3 IIR filter structures of reverberator: (*a*) The structure of comb filter. The parameter b_p is the gain of absorbent lowpass filter and g_i is the gain of comb filter. (*b*) The structure of ten parallel comb filters and three-layer nested allpass filters. (*c*) The structure of nested allpass/comb reverberator in conjunction with the early reflection module obtained using the image method.

of reverberators. First, the echo density is defined in the time domain as the number of echoes per second in a room response. Kuttruff [21] derived the formula using a sphere model to estimate the number of echoes within time t

$$N_t = \frac{4\pi(ct)^3}{3V} \tag{3}$$

where c is the speed of sound and V is the volume of room. Differentiating Eq. (3) with respect to time t gives the echo density

$$D_t = \frac{dN_t}{dt} = \frac{4\pi c^3}{V}t^2 \tag{4}$$

Note that echo density is proportional to the square of time. The second statistic is the modal density defined in the frequency domain as the number of normal modes per Hertz. The number of normal modes N_f below frequency f, independent of the room geometry, can be estimated using the following formula [21]

$$N_f = \frac{4\pi V}{c^3}f^3 + \frac{\pi S}{4c^2}f^2 + \frac{L}{8c}f \tag{5}$$

where S is the area of all walls and L is the sum of all edge lengths of the room. Differentiating Eq. (11) with respect to time leads to the expression of modal density

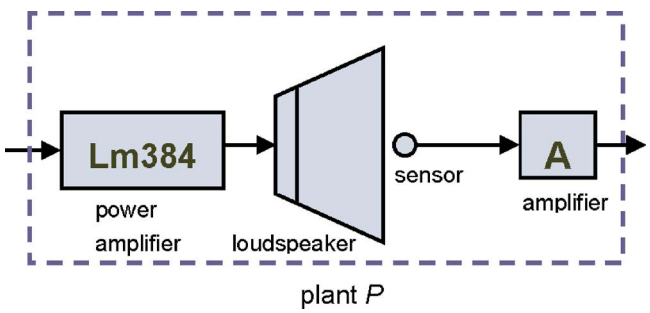

Fig. 4 The open-loop system including a headset, an embedded capacitive microphone, and a power amplifier circuit

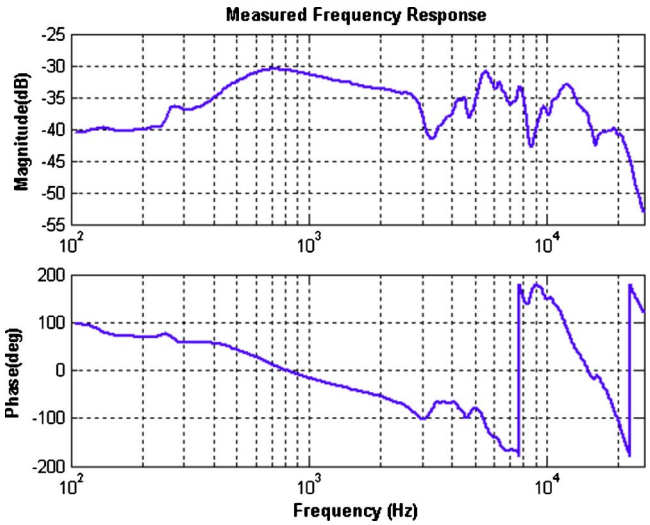

Fig. 5 The measured frequency response of the plant between 100 kHz and 25.6 KHz

$$D_f = \frac{dN_f}{df} \approx \frac{4\pi V}{c^3} f^2 \tag{6}$$

Hence, the modal density of a room grows in proportion to the square of frequency. Third, the reverberation time T_{60} is defined as the time required for the sound pressure level to drop by 60 dB after a steady-state source is switched off. Reverberation time can be estimated by Sabine's formula [22]

$$T_{60} = \frac{0.163 \cdot V}{\sum_i a_i S_i} \tag{7}$$

where V is the volume of the room; and S_i and a_i are the surface area and the associated absorption coefficient. Reverberation time is proportional to the volume of the room and inversely proportional to the wall absorptivity and the interior surface area of the room. Because most materials become more absorptive at high frequencies, reverberation time decreases as the frequency increases.

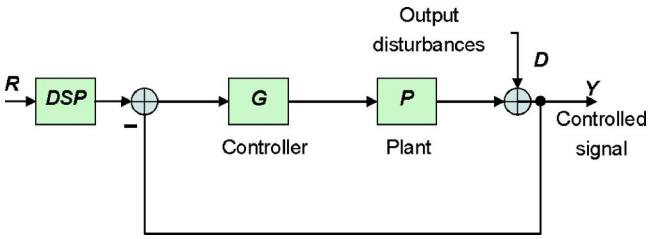

Fig. 6 The block diagram of the active headset system. The unity-feedback system is the QFT-based ANC module, whereas the feedforward system is the 3D spatial audio module.

There are two commonly used methods for predicting the early reflection of a room: the ray-tracing method and the image-source method [23,24]. The ray-tracing method is based on the assumption that sound behaves like rays in high frequencies. The distribution of sound field is determined by keeping track of the ray that passes each cell position in the space. On the other hand, the image-source method models the reflections from the room boundary as the sound wave emitted by virtual sources. Although image sources can be created indefinitely, only early reflections are computed in practice by utilizing low-order image sources. This method is particularly suited to the calculation of responses of regularly shaped rooms. The image method is employed in the paper to calculate the early reflections of room responses. For a rectangular room, the number of image sources required in the calculation of the nth-order reflection can be estimated as

$$N_n = 4n^2 + 2 \tag{8}$$

The number of image sources grows with the square of n. The impulse response of the room is constructed by recording all arrivals of the impulses from the primary source and the image sources as well. The impulse response due to the image sources is an attenuated and delayed version of the response due to the primary source. The resulting sum of impulses serves as the coefficients of the FIR filter for the early reflections of the room response. Figure 2 illustrates the impulse response calculated using

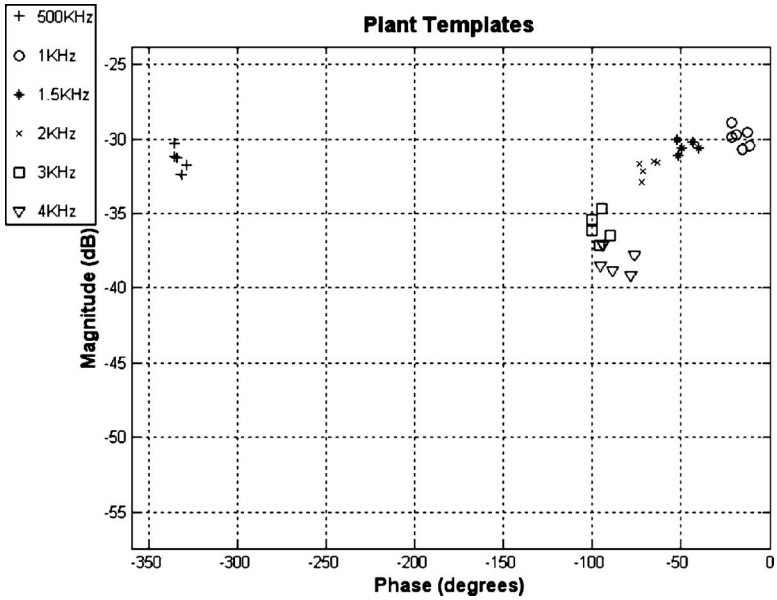

Fig. 7 Nichols chart of the plant templates measured at frequencies 500, 1 kHz, 1.5 kHz, 2 kHz, 3 kHz, and 4 kHz.

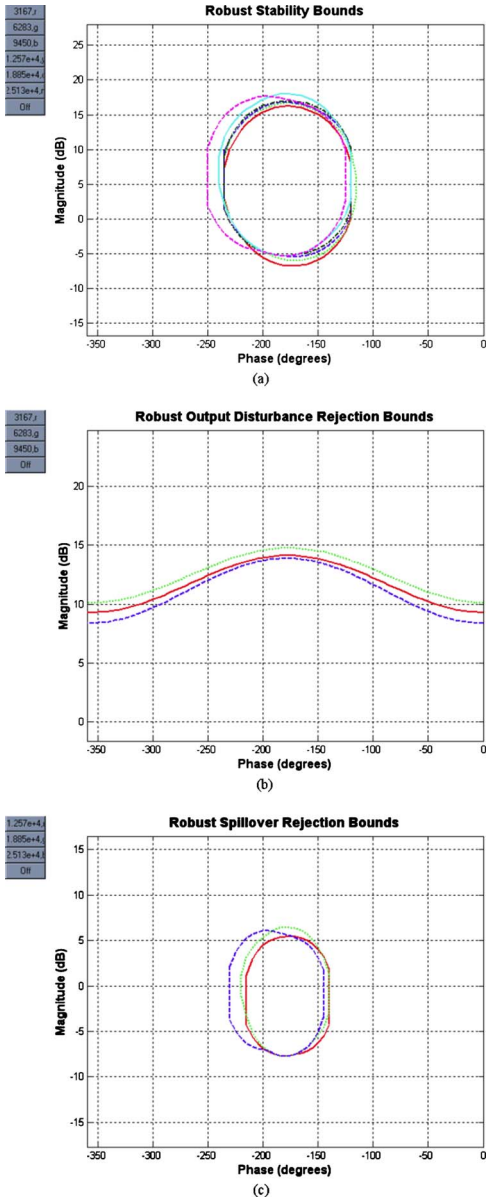

Fig. 8 QFT bounds at several frequencies, indicated with different colors. The frequencies are indicated in the legend at the top left corner. (*a*) Robust margin bounds at frequencies 500, 1 kHz, 1.5 kHz, 2 kHz, 3 kHz, 4 kHz. (*b*) Robust output disturbance rejection bounds at frequencies 500, 1 kHz, 1.5 kHz. (*c*) Robust spillover rejection bounds at frequencies 2 kHz, 3 kHz, 4 kHz.

the image-source method up to the 30th-order reflection.

In addition to the early reflection, the late reverberation is required to complete the room response. Referring to Fig. 3, the method we used for synthesizing the late reverberation is a comb filter and all-pass filter network [25]. The parallel comb filters serve to increase modal density and echo density, wheras series allpass filters serve to further increase echo density of reverberation. The filter parameters are dependent on the modal density and echo density associated with a particular room. The feedback gains g_i of the comb filters can be chosen according to a desired reverberation time [26]

$$g_i = 10^{-3m_i F_s/T_{60}} \tag{9}$$

The absorbent filter in Fig. 3(*a*) is a first-order low-pass filter whose parameters are determined by the ratio α of the reverberation times at the Nyquist frequency and dc [27]. The gain of the absorbent filter b_p is given as [26]

$$b_p = 1 - \frac{2}{1 + g^{[1-(1/\alpha)]}} \tag{10}$$

The network structure comprising ten parallel comb filters and three-layer nested allpass filters is shown in Fig. 3(*b*). Figure 3(*c*) shows the complete network structure of the nested allpass/comb reverberator, combined with the early reflection designed using the image-source method. More details of the design procedure of the reverberator network can be found in Ref. [28].

4 ANC Design Based on the QFT

This section begins with the ANC design for the headset using the QFT technique. The design procedure is carried out with the aid of the MATLAB QFT TOOLBOX [29]. A QFT procedure typically involves three basic steps: (1) computation of QFT bounds; (2) design of the controller; and (3) detailed analysis of the design.

The QFT design, performed in the frequency domain, follows very closely the classical loop-shaping designs using Bode plots. One of the design goals is to meet the performance specifications in the presence of plant uncertainties (robust performance). Prior to the design, plant frequency response templates with uncertainty models must be generated. For the plant templates, the QFT converts the closed-loop magnitude specifications into the magnitude and phase constraints, the QFT bounds, on a nominal open-loop function. A nominal open-loop function is then designed to satisfy its QFT bounds, as well as to achieve nominal closed-loop stability. The detailed procedure is given as follows.

4.1 Plant Model. One of the advantages of the QFT is that only frequency response of the plant is needed for the design. It is generally easier to measure the frequency responses than to establish an analytical transfer function model for complex systems. For the headset in Fig. 4, the plant P considered herein is defined as the system between the loudspeaker of the headset with an amplifier (the actuator) and an embedded microphone (the sensor). Several frequency responses of the open-loop plant are measured. Here, in Fig. 5, one of the frequency responses from 100 Hz to 25.6 kHz, measured by properly wearing the headset, is taken as the nominal plant. On the other hand, the difference between the other wearing scenarios (including improper ways) and the nominal plant is considered as uncertainty. For this plant, a unity-feedback controller along with a feedforward controller is employed as the control structure for our problem, as shown in Fig. 6.

4.2 Design Specifications. The first specification to be met in the control design is *robust stability*. We seek to design a controller $G(s)$ such that the closed-loop transfer function, or the *complementary sensitivity* function, satisfies

$$\left| \frac{P(j\omega)G(j\omega)}{1 + P(j\omega)G(j\omega)} \right| \leqslant 1.2, \quad \omega \geqslant 0 \tag{11}$$

With this design, a 50 deg lower phase margin and 4.4 dB lower gain margin can be attained, according to the following formulae [30]

$$\text{lower gain margin} = 1 + W_s^{-1}$$

$$\text{lower phase margin} = 180 \text{ deg} - \theta, \theta = \cos^{-1}(0.5W_s^{-1} - 1)$$

$$\in [0,180 \text{ deg}]$$

where W_S is a constraint bound index.

We place more emphasis on performance requirement on noise

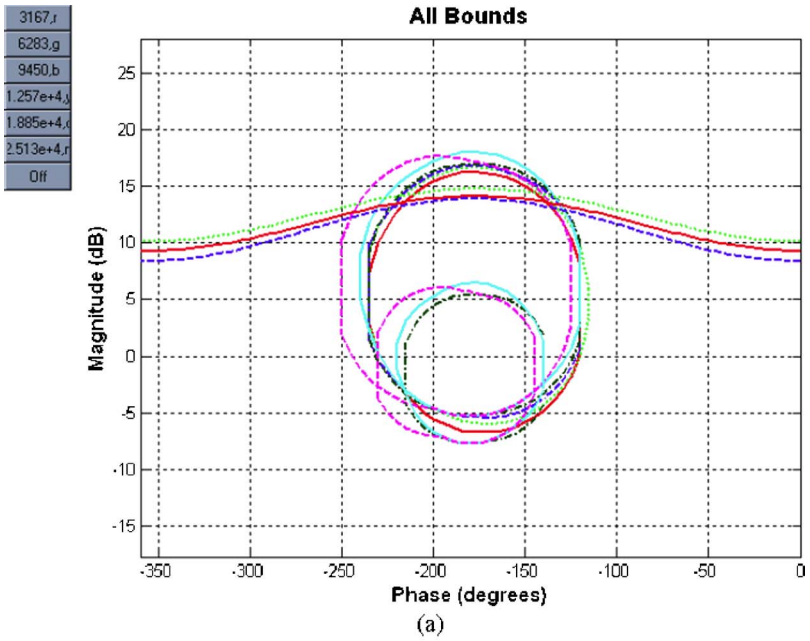

Fig. 9 QFT loop-shaping on the Nichols chart: (*a*) superposition of all bounds; (*b*) worst-case among all bounds

reduction by using a high-pass weighting filter described by Eq. (12), with the bandwidth ranging from 500 Hz to 2 kHz. We wish to achieve 10 dB reduction by this design. The specification is *robust output disturbance rejection*, described by the *sensitivity* function [30,31]. In the paper, a high-pass filter is chosen as the constraint bound

$$\left|\frac{Y}{D}(j\omega)\right| = \left|\frac{1}{1+P(j\omega)G(j\omega)}\right| \leq \left|1.1712 \times \frac{(j\omega)^3 + 26{,}700(j\omega)^2 + 2.051 \times 10^8(j\omega) + 4.44 \times 10^{11}}{(j\omega)^3 + 58{,}300(j\omega)^2 + 8.741 \times 10^8(j\omega) + 1.04 \times 10^{12}}\right|$$

$$\omega \in [500{,}2000]\ \text{Hz} \tag{12}$$

However, spillover will also arise in the band 2–5 kHz due to the performance requirement by Eq. (12). Thus, the controller is designed to ensure the spillover does not exceed 4.6 dB in the band from 2 kHz to 5 kHz. Hence, the third control specification

is *spillover rejection*, which constrains spillover at a specified frequency band. The specification of spillover rejection chosen for our problem is

$$\text{Spillover rejection} \leqslant 1.7(4.6\ \text{dB}),\ \omega \in (2000,5000]\ \text{Hz} \tag{13}$$

4.3 Plant Templates. The term plant template refers to the collection of measured frequency responses at a given frequency of the system subject to uncertainties. In the QFT design, we have to select a frequency array for computing plant templates and bounds as explained below. In considering the design bandwidth of our case, frequency array 500, 1 kHz, 1.5 kHz, 2 kHz, 3 kHz, 4 kHz are chosen. The plant templates at frequency array are shown in the Nichols chart of Fig. 7 along with their boundary. One of these templates is designated as the nominal plant in the subsequent QFT design.

4.4 Working With Bounds. Using the plant templates, the QFT converts closed-loop magnitude specifications into magnitude and phase constraints, or the QFT bounds, on a nominal open-loop function in the Nichols chart. The Nichols chart displays complex frequency response functions in terms of their magnitude (in dB) and phase (in degrees). A nominal open-loop function (GP) is then designed to satisfy these bounds and to achieve robust stability. The margin bounds at frequencies 500, 1 kHz, 1.5 kHz, 2 kHz, 3 kHz, 4 kHz are shown in Fig. 8(*a*). Next QFT design focuses on the robust performance of the closed-loop system in the band 500–2000 Hz. The robust output sensitivity bounds at frequencies 500, 1 kHz, 1.5 kHz are shown in Fig. 8(*b*). Finally, the bounds for the robust spillover rejection are shown in Fig. 8(*c*) for several frequencies within the desired performance bandwidth [2000, 5000] Hz. Superposition of all bounds is shown in Fig. 9(*a*). In general, when the problem involves more than one set of bounds, one should compute the worst-case bound as shown Fig. 9(*b*) of all sets, i.e., the intersection of all bounds, which is easier to work with than with a collection of bounds.

4.5 Loop Shaping and Analysis. Having computed the stability and performance bounds, the next step in a QFT design involves the loop shaping of a nominal open-loop function (GP) that meets the previously found bounds. The QFT design provides such an interactive environment for loop shaping in the Nichols chart. The nominal open-loop response and the associated bounds are drawn in Fig. 10(*a*). We are seeking to design a nominal loop function $L_0(s)=P_0(s)G(s)$, where $P_0(s)$ is the nominal plant, that shall attain the aforementioned specifications. In words, loop

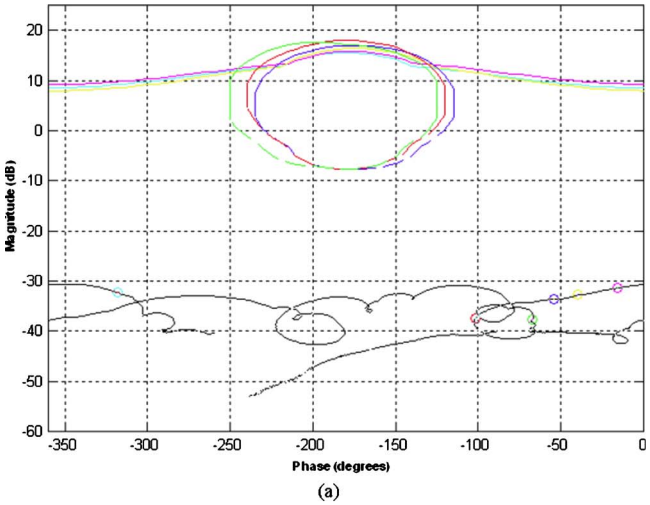

Fig. 10 Nichols chart of the open-loop response $G(s)P(s)$: (*a*) uncompensated open-loop response and its bounds; and (*b*) compensated open-loop response with a sixth-order controller

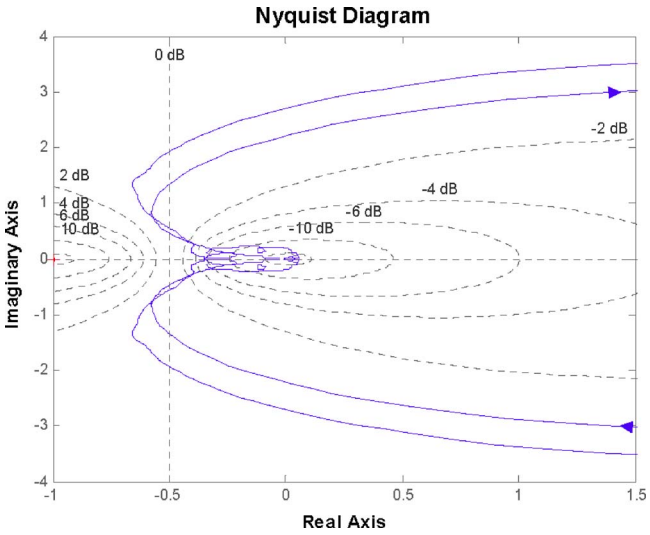

Fig. 11 Nyquist diagram of the open-loop system $G(s)P(s)$

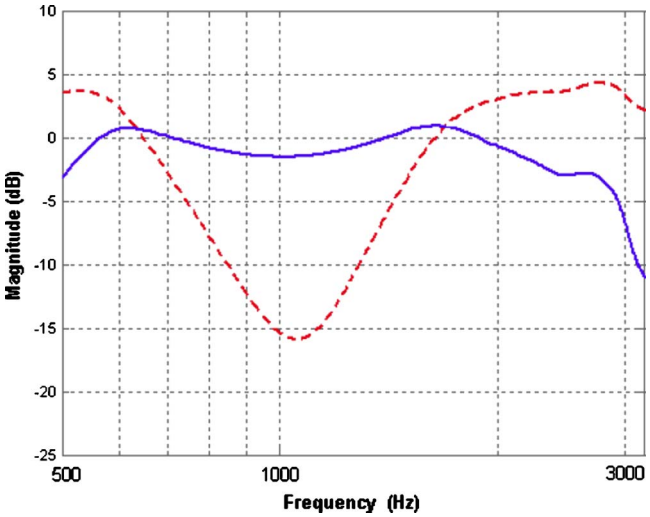

Fig. 12 The sensitivity function (dashed line) and the complementary sensitivity function (solid line)

shaping involves adding poles and zeros until the nominal loop lies near its bounds and results in nominal closed-loop stability. The QFT procedure enables the users to consider different controller complexities and weigh possible tradeoffs. The controller $G(s)$ is designed by adding poles and zeros in the Nichols chart to satisfy the aforementioned specifications. The result after loop shaping is shown in Fig. 10(*b*).

In the present design, robust stability has been achieved since the nominal loop does not violate the robust margin bounds and does not cross the ray [32]

$$R = \{(\phi, \gamma):\ \phi = -180 \text{ deg},\ \gamma > 0 \text{ dB}\} \tag{14}$$

The feedback controller resulted from the interactive QFT designed is given by the following sixth-order transfer function

$$G(s) = 0.7882 \times \frac{\left(\frac{s}{216}+1\right)\left(\frac{s^2}{7233^2}+\frac{2\times 0.8421}{7233}s+1\right)\left(\frac{s^2}{2.699e4^2}+\frac{2\times 0.7202}{2.699e4}s+1\right)}{\left(\frac{s^2}{6708^2}+\frac{2\times 0.1797}{6708}s+1\right)\left(\frac{s^2}{6720^2}+\frac{2\times 0.2885}{6720}s+1\right)\left(\frac{s^2}{2.422e4^2}+\frac{2\times 0.1665}{2.422e4}s+1\right)} \tag{15}$$

For the design, it is advisable to check if the close-loop system is stable by using the Nyquist plot as shown in Fig. 11. It is concluded that the closed-loop system is stable because the frequency response curve does not encircle the critical point $(-1,0)$.

The sensitivity function (the dotted line) and the complementary sensitivity function (solid line) pertinent to the present design are shown in Fig. 12. The results reveal that the performance is attained within 700–2 kHz, and the spillover rejection is also satisfied within 2 K–5 kHz.

5 Experimental Verification

5.1 ANC Performance. Hardware was implemented to integrate the above-mentioned 3D spatial audio and ANC into a single unit. First, the QFT-based active feedback controller is realized by using analog circuits because, after preliminary evaluation, we found that the delay of the DSP is much too large to afford a digital design. The analog circuits of the sixth-order controller as designed previously can be easily implemented using operational amplifiers (OPs), following the design method of active biquad filters [33]. The resulting circuit of the feedback controller $G(s)$ is shown in Fig. 13. Figure 14 shows the implemented frequency response of the QFT controller (solid line) that compares quite well in the control bandwidth to the designed response (dotted line).

To assess the performance of the ANC, the headset was worn by an acoustic manikin. A 2 in. condenser microphone was instru-

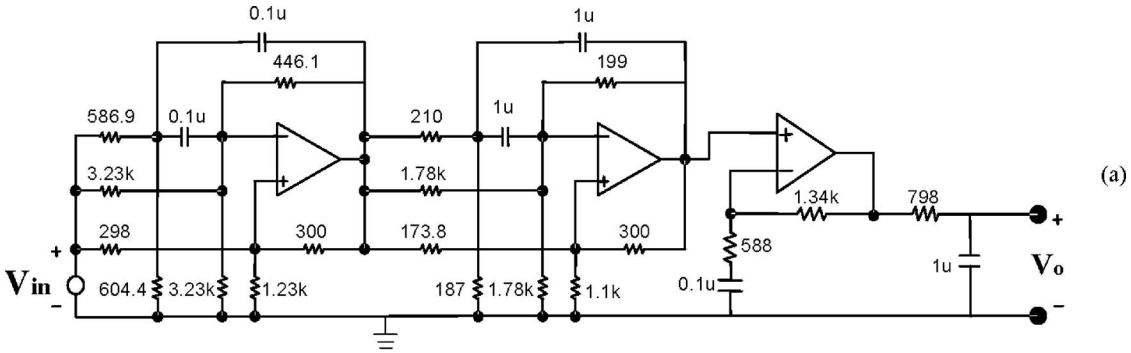

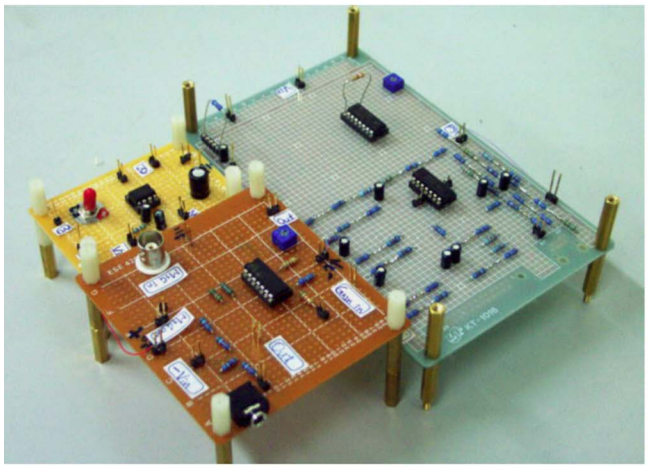

(b)

Fig. 13 The QFT-based active noise canceller: (*a*) circuit diagram; (*b*) photo

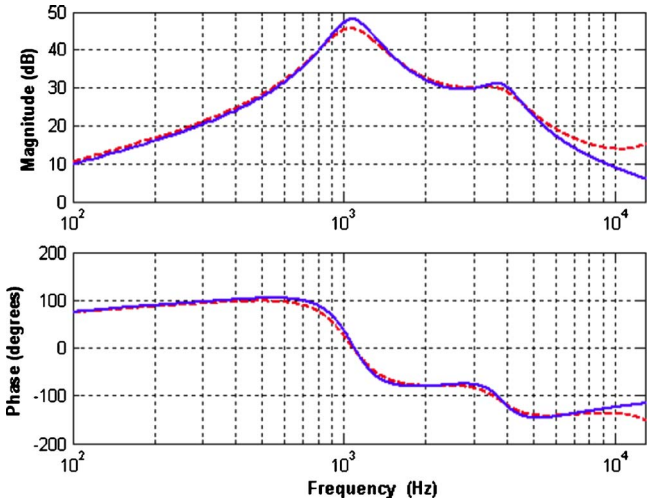

Fig. 14 Frequency response functions of the feedback controller: (solid line) designed; (dashed line) implemented

mented in the ear canal of the manikin. A 3.5 in. full range loudspeaker positioned 1 m away from the manikin, playing white noise, served as the extraneous noise source. The test was conducted inside an anechoic chamber. The sound pressure responses measured by the microphone with and without active control are compared in Fig. 15(*a*). Noise attenuation was achieved in the band 700–1700 Hz. The maximal attenuation reached 13 dB in the band. These results compare quite well with those predicted by the sensitivity functions shown in Fig. 15(*b*).

5.2 Subjective Listening Test of the Integrated System. A listening test was carried out to examine the total system that integrated the 3D spatial audio and the ANC. A feedforward module that implements the 3D audio effects was realized by using a fixed-point DSP, ADI BF-533. The 3D audio effects considered herein are the aforementioned HRTF and the reverberator. The feedforward 3D audio module was connected to the previously mentioned analog feedback ANC module to form a hybrid control system (Fig. 6). To assess the proposed system, subjective listening experiments were conducted. Six subjective indices including sound image definition, spaciousness, ambience, clarity, naturalness, and externalization are selected for the listening tests. Ten subjects took part in the test. Listeners' perception in terms of the subjective indices was answered in a questionnaire on a scale ranging from −5 to 5. The 3D audio presentation without ANC was taken as the benchmark. The grade 0 indicates "no difference" between the audio presentation under test and the uncontrolled benchmark. A grade greater/less than zero indicates that the controlled/uncontrolled signal perceptually outperforms the uncontrolled/controlled signal, in terms of a particular subjective index. Figure 16 illustrates the result of the subjective listening test in which the average grades for each index are summarized. It is evident from the result that the 3D audio-ANC headset performed well in all indices (with all positive grades), as compared to the headset with no ANC. As anticipated, the grade of *clarity* was not as high as the other indices since the reverberator in the 3D module would adversely affect this particular aspect. To further assess the significance of the result, an ANOVA test was conducted. Table 1 shows the result of the ANOVA test. It is interesting to note that the significance value of *clarity* is above the commonly chosen threshold of 0.05, indicating the grade in this aspect was somewhat disputed. But, overall, the difference made by the new system is statistically significant, as revealed by the fact that the significance values shown in Table 1 are mostly well below the threshold of 0.05. It is then concluded from the

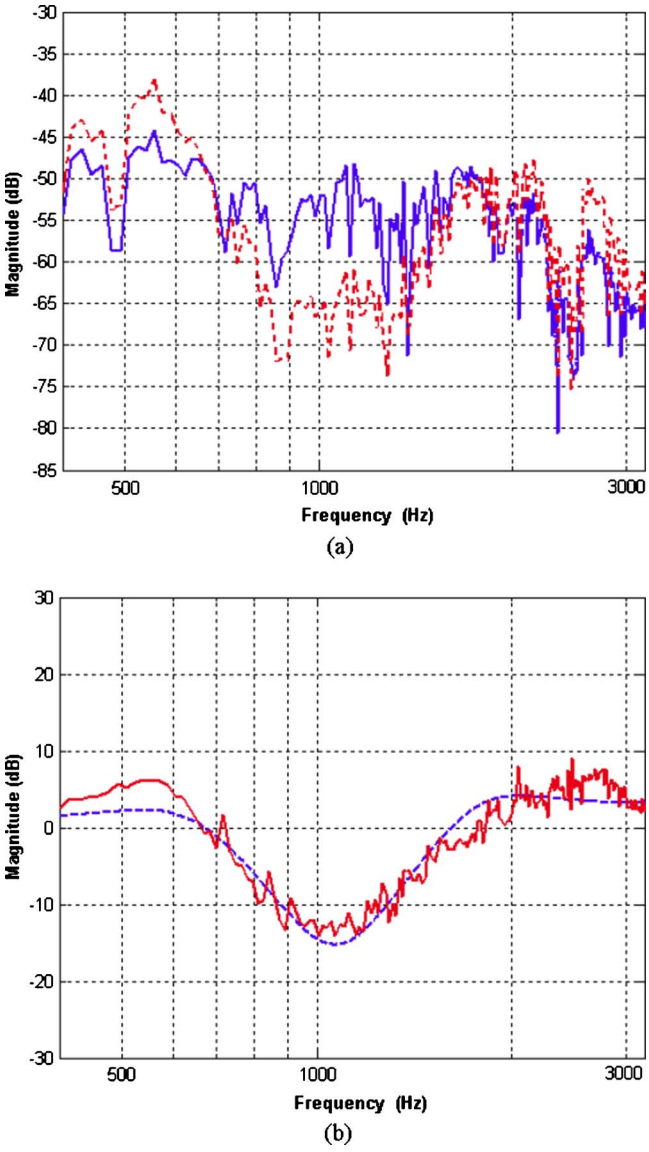

Fig. 15 Results of the active noise cancellation: (*a*) sound pressure spectra measured by the microphone with (dashed line) and without (solid line) the active control; and (*b*) sensitivity function; (solid line) measurement; (dashed line) simulation

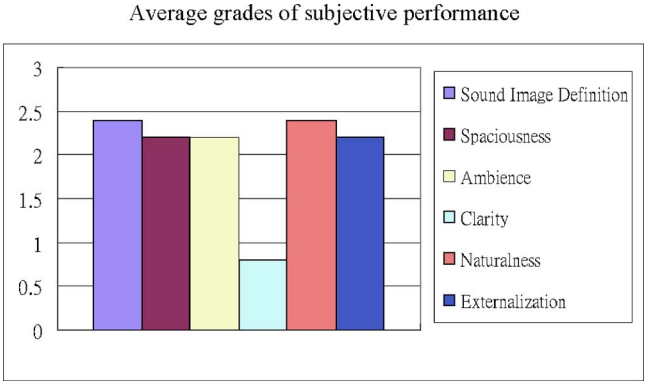

Fig. 16 The average grades of subjective indices obtained from the listening test

Table 1 Significant values of the ANOVA test on the listening experiment

Subjective index	Significance value
Sound image definition	9.8834e−6
Spaciousness	4.1488e−6
Ambience	4.1488e−6
Clarity	1.4111e−1
Naturalness	1.5280e−3
Externalization	3.7011e−4

results that the ANC proved to be useful in enhancing 3D spatial sound reproduction by using a headset.

6 Conclusions

A headset that integrates the QFT-based ANC and 3D spatial audio processing technologies has been proposed in the paper. It is demonstrated that active control approaches can be used to enhance the performance of 3D audio. As pointed out by the reviewer, some examples of active control from the recent JVA publications are also along this line [34,35]. The active noise canceller was designed by using the QFT loop-shaping technique which yielded a feedback controller with various control performance and robustness specifications taken into account. The low-order controller was implemented by using analog circuits to minimize the loop delay. Noise attenuation was achieved in the band 700–1700 Hz. The maximal attenuation reached 13 dB in the band.

The feedback ANC and the feedforward 3D audio are then integrated into the headset. It is observed from the result that the combined system performed well in all indices, as compared to the headset with no ANC. In addition, the difference made by the combined system is statistically significant, as revealed by the fact that the significance values shown in the AVOVA test are mostly well below the threshold of 0.05. It is then concluded from the results that the ANC proved to be useful in enhancing 3D spatial sound reproduction by using a headset.

Acknowledgment

The work was supported by the National Science Council (NSC) in Taiwan, under Project No. NSC 92-2212-E009-030.

References

[1] Horowitz, I. M., 1963, *Synthesis of Feedback Systems*, Academic, New York.
[2] Horowitz, I. M., and Sidi, M., 1972, "Synthesis of Feedback Systems With Large Plant Ignorance for Prescribed Time-Domain Tolerances," Int. J. Control, **16**(2), pp. 287–309.
[3] Horowitz, I. M., 1992, *Quantitative Feedback Theory (QFT)*, QFT Publications, Boulder, CO.
[4] Gardner, B., and Martin, K., 1994, "HRTF Measurements of KEMAR Dummy-Head Microphone," MIT Media Lab, http://sound.media.mit.edu/KEMAR.html
[5] Batteau, D. W., 1967, "The Role of the Pinna in Human Localization," Proc. R. Soc. London, Ser. B, **168**, pp. 158–180.
[6] Batteau, D. W., 1968, *Listening with the Naked Ear: The Neuropsychology of Spatially Oriented Behavior*, Dorsey Press, Homewood, IL.
[7] Wright, D., Hebrank, J. H., and Wilson, B., 1974, "Pinna Reflections as Cues for Localization," J. Acoust. Soc. Am., **56**(3), pp. 957–962.
[8] Algazi, V. R., Duda, R. O., Thompson, D. M., and Avendano, C., 2001, "The CIPIC HRTF Database," *Proceedings IEEE Workshop on Applications of Signal Processing to Audio and Electroacoustics*, Avignon, August 1988, Mohonk Mountain House, New Paltz, NY, pp. 99–102, http://interface.cipic.ucdavis.edu/
[9] Lueg, P., 1936, "Process of Silencing Sound Oscillations," US Patent No. 2,043,416.
[10] Bai, M., and Lee, D., 1997, "Implementation of an Active Headset by Using the H_∞ Robust Control Theory," J. Acoust. Soc. Am., **102**(4), pp. 2184–2190.
[11] Elliott, S. J., Stothers, I. M., Nelson, P. A., McDonald, A. M., Quinn, D. C., and Saunders, T., 1988, "The Active Control of Engine Noise Inside Cars," *Proceedings Inter-noise*, San Diego, CA, pp. 987–990.
[12] Dorling, C. M., Eatwell, G. P., Hutchins, S. M., Ross, C. F., and Sutcliffe, S. G. C., 1989, "A Demonstration of Active Noise Reduction in an Aircraft Cabin," J. Sound Vib., **128**(2), pp. 358–360.
[13] Elliott, S. J., and Nelson, P. A., 1994, "Active Noise Control," Noise News Int., **2**, pp. 75–98.
[14] Tohki, M. O., and Leitch, R. R., 1992, *Active Noise Control*, Clarendon, Oxford, UK.
[15] Fuller, C. R., and von Flotow, A. H., 1995, "Active Control of Sound and Vibration," IEEE Control Syst. Mag., **15**(6), pp. 9–19.
[16] Nelson, P. A., and Elliott, S. J., 1992, *Active Control of Sound*, Academic, New York, NY.
[17] Elliott, S. J., 2001, *Signal Processing for Active Control*, Academic, New York, NY.
[18] Olson, H. F., and May, E. G., 1953, "Electronic Sound Absorber," J. Acoust. Soc. Am., **25**, pp. 1130–1136.
[19] Wheeler, P. D., 1986, "Voice Communication in the Cockpit Noise Environment—The Role of Active Noise Reduction," Ph.D. thesis, University of Southampton, Southampton, UK.
[20] Gay, S. L., and Benesty, J., 2000, *Acoustic Signal Processing for Telecommunication*, Kluwer Academic, Boston, MA.
[21] Kuttruff, H., 1991, *Room Acoustics*, Elsevier, New York, NY.
[22] Sabine, W. C., 1972, "Reverberation," *Acoustics: Historical and Philosophical Development*, R. B. Lindsay, ed., Dowden, Hutchinson, and Ross, Stroudsburg, PA.
[23] Savioja, L., 1999, "Modeling Techniques for Virtual Acoustics," Doctorate thesis, Helsinki University of Technology, Espoo, Finland.
[24] Lehnert, H., and Blauert, J., 1992, "Principles of Binaural Room Simulation," Appl. Acoust., **36**, pp. 259–291.
[25] Gardner, W. G., 1992, "The Virtual Acoustic Room," Master's thesis, MIT Media Lab, Cambridge, MA.
[26] Frenette, J., 2000, "Reducing Artificial Reverberation Requirements Using Time-Variant Feedback Delay Networks," Master Research Project, University of Miami, Miami, FL.
[27] Beltra'n, F. A., and Beltra'n, J. R., 2002, "Implementing Reverberation Algorithms in Matlab," J. New Music Res., **31**, pp. 153–161.
[28] Bai, M. R., and Bai, G., 2007, "Optimal Design and Synthesis of Reverberators with a Fuzzy User Interface for Spatial Audio," J. Audio Eng. Soc., in press.
[29] Borghesani, C., Chait, Y., and Yaniv, O., 2003, *the QFT Frequency Domain Control Design Toolbox User's Guide*, Terasoft, US.
[30] Chait, Y., and Yaniv, O., 1993, "Multi-Input/Single-Output Computer Aided Control Design Using the Quantitative Feedback Theory," Int. J. Robust Nonlinear Control, **3**, pp. 47–54.
[31] Chait, Y., Borghesani, C., and Zheng, Y., 1995, "Single-Loop QFT Design for Robust Performance in the Presence of Non-Parametric Uncertainties," J. Dyn. Syst., Meas., Control, **117**, pp. 420–424.
[32] Cohen, N., Chait, Y., Yaniv, O., and Borghesani, C., 1994, "Stability Analysis Using Nichols Charts," Int. J. Robust Nonlinear Control, **4**, pp. 3–20.
[33] Chen, W. K., 1986, *Passive and Active Filters: Theory and Implementations*, Wiley, New York, NY.
[34] Yuan, J., 2006, "Active Resonators for Noise Absorption," ASME J. Vibr. Acoust., **128**(1), pp. 115–121.
[35] Bisnette, J. B., Smith, A. K., Vipperman, J. S., and Budny, D. D., "Active Noise Control Using Phase-Compensated, Damped Resonant Filters," ASME J. Vibr. Acoust., **128**(2), pp. 148–155.